An ISO Upper Limit to the Brown Dwarf Halo in the Edge-on Galaxy NGC4565

Charles Beichman, George Helou, Dave Van Buren, Ken Ganga

Infrared Processing and Analysis Center Jet Propulsion Laboratory, California Institute of Technology, Pasadena, CA

F.X. Desert

Laboratoire d'Astrophysique de l'Observatoire de Grenoble, France

Key Words: Brown Dwarfs; Galaxy Halo; Infrared; NGC 4565

1. Abstract

We present deep ISOCAM observations taken at 4.5 μm(LW1) in search of a faint halo surrounding the edge-on spiral galaxy NGC4565. Such a halo might exist if the massive halo needed to explain the flat rotation curve of this galaxy were attributable to a population of faint, red objects. The upper limit, 8.1 kJy sr^{-1} (3σ), reported here excludes a halo consisting of late M dwarfs but not of cooler, lower luminosity brown dwarf stars.

2. Introduction

The dynamics of stars, galaxies and clusters of galaxies offer strong circumstantial evidence for the existence of substantial amounts of matter that exerts a gravitational influence but which is not apparent at visible wavelengths. Progress has been made in identifying the nature of the halo material. The direct detection of dark matter in the halo of the Milky Way (Alcock *et al.* 1997a) through gravitational micro-lensing has led to characterization of the halo population of our galaxy as low mass stars, possibly white dwarfs stars. Sackett *et al.* 1994 detected faint light in a halo around NGC 5907 on a scale large enough to account the flat rotation curve seen in that galaxy. The colors of that faint halo (Rudy *et al.* 1997) are consistent with a mixed population of very red stars.

But direct results on galactic halos are few and arguments continue about the nature of the dark matter. A possible refuge for baryonic dark matter is faint red stars at or below the low mass cutoff of the main sequence. A cloud of brown dwarfs could have escaped detection at visible wavelengths yet, if present in sufficient number, account for the missing halo matter. As described below, simple models of a red star or brown dwarf halo suggest a 4.5 μm halo brightness of $0.2 - 10$ kJy sr^{-1} for the 3.5×10^{11} M$_\odot$ halo needed to account for the rotation curve of NGC 4565.

3. Observations

3.1. Observing Strategy

3.1.1. Choice of Galaxy

We selected the edge-on galaxy NGC 4565 (Table 1) out of an extensive list of edge-on galaxies available in the NASA Extragalactic Database (NED). Selection criteria included high ecliptic and galactic latitude and low 60 and 100 μm cirrus on the IRAS images. The galaxy NGC 5907 also met these criteria but was observed as part of the ISO Guaranteed time for this same project. NGC 4565 has a flat rotation curve (Casterno and Van Gorkom 1991; Rupen 1991) extending over 30 kpc with an inferred total mass of dark matter of 3.5×10^{11} $M_\odot$ (see below). The radiation from the galaxy is well confined to a narrow disk, with little or no extra-planar emission seen at optical (Rand *et al.* 1992), radio (Rupen 1991), or X-rays (Vogler, Pitesch and Kahabka 1996).

3.1.2. Choice of Observational Parameters

The expected halo signal is small ($\leq$ 1 kJy sr^{-1}) compared with the zodiacal, Milky Way and host galactic foregrounds. We elected to observe using ISOCAM with the CAM03 beam-switch macro in the 4.5 μm (LW1) filter. This wavelength maximizes the contrast of the halo with respect to the zodiacal emission for star/brown dwarf masses in the range 0.02-0.2 $M_\odot$. In the LW1 filter the halo emission could be as bright as 0.1% of the zodiacal emission. At longer wavelengths, the contrast ratio with the zodiacal emission is 2 orders of magnitude worse and the experiment becomes difficult for any observatory embedded within the local zodiacal cloud at 1 AU.

An additional motivation for selecting the LW1 filter is avoidance of galactic cirrus.

There is a minimum in the emission from small particles in the 4.5 μm window, while the LW2 filter contains a number of PAH features (Bernard *et al.* 1994) that could introduce spurious Milky Way emission into the observations. The estimated cirrus brightness at 4.5 μm is $4 \times 10^{-4} \times I(100\mu\text{m})$ MJy sr^{-1} where I(100 μm) is the IRAS 100 μm intensity. In regions of weak IRAS cirrus, I(100 μm) $\sim$1 MJy sr^{-1}, the cirrus intensity at 4.5 μm should be a less than 0.4 kJy sr^{-1} with gradients across the observed region being smaller still.

Observations were made using 6″ pixels as a compromise between large field of view (180″), sensitivity to low surface brightness, and good camera operation. The predicted photon- and detector-noise-limited sensitivity expected for the observational procedure outlined below after averaging over all pixels in the array is approximately 1σ = 0.2 kJy sr^{-1}. As shown below, the final sensitivity of these observations was approximately 2.7 kJy sr^{-1}(1σ), or roughly a factor of 15 worse than expected. The degradation is due to low level drifts in detector gain and dark current due to effects of changing illumination and charged particle events.

3.1.3. Observational Sequence

The observational sequence was designed to minimize instrumental drifts and to provide spatial and temporal chopping on as many scales as possible. An observational sequence denoted here as a "scan", consisted of 1000 sec of array stabilization followed by concatenated ON-OFF pairs made at six positions along the minor axis of the galaxy, three positions symmetrically placed on either side of the galaxy. The observation at each position consisted of 5 (***TBS***) 20-sec integrations at each of: 1) the ON position; 2) at the OFF_E position displaced $\sim$40′ to the East in ecliptic coordinates; 3) at the ON position again; and 4) at the OFF_W position displaced 40′ to the West in ecliptic coordinates. The OFFs were displaced in ecliptic longitude relative to the ON position to provide a direct

monitor of the gradient of the zodiacal emission. No observation was made of NGC 4565 itself to avoid imprinting light from the galaxy onto the ISOCAM array. Filter changes were suppressed during the entire sequence of observations to minimize flux-induced responsivity changes.

The scans along the minor axis of the galaxy were repeated on four separate occasions, denoted as Scans 1, 2, 3 and 4. Small, $\sim 15''$ offsets were applied to the nominal positions to impose a dithering pattern designed to improve the flat-fielding and bad pixel rejection. To mitigate against direction dependent effects in the data or data reduction, two scans were made with the telescope stepping Northeast and two were made with the telescope stepping Southwest. Due to observing time constraints, two positions were observed only 3 instead of four times. Table 2 and Figure 1 summarize the scan strategy and the ISO observing log. The total integration time for those fields observed all four times was about 1400 sec.

3.2. Data Reduction

The data for each position within each scan were calibrated using library flat, dark, and sensitivity. Pixels with obvious glitches or point sources were rejected *** *for the duration of a scan?****. The calibrated median of all remaining pixels is shown in Figure 2 for each position within scans 1-4. It should be noted that the emission is close to that predicted by the IRAS model for the zodiacal light (Good 1994; Reach *et al.* 1995), 200 kJy sr^{-1}. However, the signals at first position in each sequence fall considerably above the remaining values. Additionally, the signal level seen in the data for the first position (ON_1, OFF_E, ON_2, OFF_W) declines with time. We conclude that there is a residual transient response even after the 1000 sec of stabilization. Examination of the difference between the first and second ON observation at each position, ON_1-ON_2 (Figure 3), confirms that the array has

not stabilized during the first set of integration

The difference OFF_E-OFF_W measures the zodiacal light gradient due to a change of about $\pm 40'$ in ecliptic latitude (more accurately cone angle with respect to the sun at the epoch of observation). The median value of the OFF_E-OFF_W differences are shown for scans 1-4 in Figure 4. The predicted level of the change, -3.5 kJy sr^{-1} on Day 184 is consistent with the measurements -5.1 ± 1.7 kJy sr^{-1}. The -4.9 ± 0.9 kJy sr^{-1} measured on day 221 is about a factor of two lower than the predicted value of -9 kJy sr^{-1}. The agreement, while not perfect, is encouraging given the uncertainties in the model as well as in correction for the various calibration effects. The uncertainties in the measurements in the zodiacal gradient serves as a valuable indicator of the uncertainties expected for the halo emission from NGC 4565.

We next formed the beam-switch differences needed to measure the halo of NGC 4565. We took two types of difference to monitor systematic effects: 1) to exclude possible transient effects in the first ON position, we calculated ON_2 minus the average of the two OFFs (crosses in Figure 5); 2) to obtain the theoretically best possible signal to noise ratio, we calculated the average of the two ON's minus the average of the two OFFs (boxes). The scan-by-scan data are shown in Figure 5.

Finally, we combined data for each sky position observed within the four scans. Since we have to ignore the first measurement in each set of observations to minimize residual transients, there are only two measurements at the two positions furthest North and South of the galaxy. For each position we find the average and sigma of the two or four measurements using both forms of the differences shown in Figure 5. The results are shown in Figure 6. The more conservative measurement (difference type #1, above) is summarized in Table 3. There is no increase in signal as one moves close to the galaxy (50 kpc vs. 12 kpc along the minor axis). We adopt 8.1 kJy sr^{-1} as the 3 σ limit to the brightness of any

galaxy halo 12 kpc away from the center of NGC 4565. This value compares favorably with halo observations of other galaxies (Gilmore and Unavane 1998). However, the rocket observations of N4565 (Bock *et al.* 1998) using more stable InSb detectors are considerably more sensitive than the observations reported here.

4. Discussion

What little is known about galaxy halos has been determined from dynamical clues (Trimble 1987; Ashman 1992): a scale length between 1-10 kpc with a maximum extent of 25-50 kpc, a total dark mass ranging from 10^7 $M_\odot$ in dwarf irregular galaxies to 10^{12} $M_\odot$ in galaxies like the Milky Way. We know little about the halo content even if it is baryonic. Detections of micro-lensing events toward the LMC (Alcock *et al.* 1993; Alcock *et al.* 1997a; Aubourg *et al.* 1993) suggest stellar or substellar objects with masses in the range 0.01-0.5 $M_\odot$, although mass of a few tenths of a solar mass are currently favored on the basis of statistical analyses of micro-lensing profiles (Alcock *et al.* 1997a). The possible detection of a halo in R band around NGC 5907 (Sackett *et al.* 1994) suggests a halo of very late M stars. Rudy *et al.* 1997 have measured the NGC 5907 halo at J and K in the near-infrared and found that a peculiar mixture of stellar types is required to fit the colors of the halo.

If red stars or substellar objects (brown dwarfs) are responsible for the halo, then their emission will be most prominent in the infrared, at a wavelength that might range from 2 μm to 60 μm depending on the mass, age and chemical composition of the objects (Stevenson 1991; Burrows *et al.* 1997).

We predict the brightness of the halo emission as follows. Let the density distribution of the halo follow that expected for an isothermal sphere with core radius, R_{core} (Bahcall

and Soneira 1980;Kent 1986):

$$\rho(r) = \frac{\rho_0}{1 + \frac{r^2}{R_{core}^2}} \tag{1}$$

where $\rho_0 = \frac{V_{max}^2}{2\pi G R_{core}^2}$ and V_{max} is the maximum velocity of the galaxy rotation curve. Then the total number of objects of a given mass, m, in a halo extending to a maximum radius, R_{max} is given by:

$$M_{Tot} = 4\pi\rho_0 R_{core}^3 \left(\frac{R_{max}}{R_{core}} - tan^{-1} \frac{R_{max}}{R_{core}} \right) \tag{2}$$

The surface brightness of the halo at a given impact parameter, βR_{max}, is given by

$$I_\nu(\beta) = \pi a^2 B_\nu(T) N(\beta) \tag{3}$$

where $N(\beta)$ is the column density of objects assumed to be emitting as blackbodies of radius a. While the spectrum of a brown dwarf can deviate strongly from that of a blackbody at wavelengths around 1-2 μm due to molecular absorption by methane and other species (Marley *et al.* 1997; Geballe *et al.* 1996), at the longer wavelengths considered here the blackbody approximation should not be greatly in error. Figures 12-14 of Burrows *et al.* 1997 show the 4-5 μm spectrum to be relatively free of significant absorption.

The column density at impact parameter $\beta \mathrm{R}_{max}$, $N(\beta)$ is given by

$$N(\beta) = 2n_0 \beta R_{max} \int_0^{\theta_{max}} \frac{1}{\gamma^2 + cos^2\theta} \tag{4}$$

$$= \frac{2n_0 R_{core}}{\sqrt{(1+\gamma^2)}} tan^{-1} \left(\frac{R_{max}}{R_{core}} \frac{\sqrt{(1-\beta^2)}}{\sqrt{(1+\gamma^2)}} \right)$$

where $\gamma = \beta R_{max}/R_{core}$ and $\theta_{max} = \cos^{-1}\beta$. For a population of objects with a single mass, m_*, the central number density of objects, $n_0 = \rho_0/m_*$. The modification of the above for power-law distributions of stars (or brown dwarfs) of various masses is straightforward. We examine five cases:

- Red stars taken to be M8 stars with $M_* = 0.2\mathrm{M}_\odot$, $\log(\mathrm{L}_*) = -2.2$, T_{eff}= 2400 K
- Old (10^{10} yr) brown dwarf stars with $M_* = 0.07$ $\mathrm{M}_\odot$, $\log(\mathrm{L}_*) = -5.25$, at T_{eff}=880 K (Stevenson 1991, Burrows *et al.* 1997).
- A mixed red-star, brown dwarf model with a continuous power-law distribution with $\alpha = -1$ where $dN(m)/dM \propto m^{-\alpha}$ extending from 0.2 $\mathrm{M}_\odot$ to 0.02 $\mathrm{M}_\odot$.
- A brown dwarf-only model with $\alpha = -1$ and extending from 0.07 $\mathrm{M}_\odot$ to 0.02 $\mathrm{M}_\odot$.
- A white dwarf model with M=0.7 $\mathrm{M}_\odot$, $\log(\mathrm{L}_*)$=-2.5 $\mathrm{L}_\odot$, and T=8000 K. This model is included since white dwarfs are a favored constituent of the Milky Halo (Alcock *et al.* 1997a; Alcock *et al.* 1997b; Graff *et al.* 1998).

To evaluate the emission from a stellar or brown dwarf halo we need estimates of the halo mass, M_{halo}, the core radius, and the maximum extent. Ashman 1992 quotes an empirical relation between the core radius and the luminosity of the galaxy derived by Kormendy 1990 $R_{core} = 5.9(\frac{L_B}{10^9 L_\odot})^{0.34}$ kpc. With $L_B = 3.7 \times 10^{10}\mathrm{L}_\odot$(e.g. Rupen 1991, $R_{core} \sim 18$ kpc. From HI (Rupen 1991 we find $V_{max} = 275$ km s^{-1}. With the arbitrary assumption of $R_{max} = 50$ kpc and application of Eqns (1) and (2), we derive a total halo mass of $3.5 \times 10^{11}\mathrm{M}_\odot$.

The variation of brightness can be derived using Eqns. (3) and (4) for the various models (Table 4). Figure 7 shows the results of the model calculations along with the observational limits at 12, 20, and 50 kpc. Also included is the surface brightness observed

along the minor axis in the visible (Näslund and Jörsäter 1997); the values are extrapolated to 4.5 μm using the colors of an M star (V-M $\sim$ 3.3 mag).

Both the ISO and extrapolated visible light observations rule out the presence of a stellar halo consisting of hydrogen burning red dwarf stars. The ISO data are not sensitive enough to constrain models consisting only of the brown (or white) dwarfs. The conclusion that red stars do not form the halo is also consistent ground-based near-IR observations toward NGC 100 (Casali and James 1995) and with HST observations of the halo of the Milky Way (Flynn *et al.* 1996). While numerous dynamical models (Chabrier, Segretain, and Mera 1996; Alcock *et al.* 1997b;Gyuk, Evans and Gates 1998) argue against brown dwarfs comprising the major part of galaxy halos, additional observations with dedicated rocket observations (Bock *et al.* 1998), the WIRE satellite, or with SIRTF will be needed to determine definitively whether substellar objects (isolated, or in clusters (Kerins 1998) play any role in forming halos of galaxies.

5. Acknowledgements

CAB would like to acknowledge the hospitality of Jean-Loup Puget and the Institut d'Astrophysique Spatiale (Orsay, France), and of the Dominion Radio Astrophysical Observatory (Penticton, Canada). This work was funded by an ISO grant from NASA. IPAC is operated for NASA by JPL and California Institute of Technology under a contract with Caltech.

REFERENCES

Ashman, K.M. 1992, *P.A.S.P.*, **104**, 1109.

Alcock, C. *et al.* 1993, *Nature*, **365**, 621.

Alcock, C. *et al.* 1997, *Ap. J.*, **479**, 119.

Alcock, C. *et al.* 1997, *Ap. J.*, **486**, 697.

Aubourg *et al.* 1993, *Nature*, **365**, 623.

Bahcall, J. N.and Soneira, R. M. 1980, *Ap. J. (S)*, **44**, 73.

Bernard, J-P., Boulanger, F., Desert, F.X. and Girard, M., Helou, G. and Puget, J-L, 1994, *Astron & Ap.*, **291**, L5.

Bock, J.J., Langer, A.E., Yost, S.A., Uemizu, K., Kawada, M., Matsumoto. T. 1998, *Bull. Am. Astr. Soc*, **192**, 7006.

Burrows, A. *et al.* , 1997, *Ap. J.*, **491**,856.

Casali, M.M. and James, P.A. *M.N.R.A.S.*, **274**, 709.

Casertano, S. and Van Gorkom, J. 1991, *A. J.*, **101**, 1231.

Chabrier,G. Segretain, L. and Mera, D. 1996, *Astron & Ap.*, bf 468, 21.

Engargiola, G. and Harper, D.A, 1992, *Ap. J.*, **394**, 104.

Flynn, C., Gould, A., Bahcall, J.N., 1996, *Ap. J.*, *466*, L55.

Geballe *et al.* 1996, *Ap. J.*, **467**, L101.

Gilmore, G. and Unavane, M. , 1998, abstract submitted to ISO Conference.

Good, J. 1994, in *The Explanatory Supplement to the IRAS Infrared Sky Survey Atlas.*

Graff, D.S., Laughlin, G., Freese, K., 1998, *Ap. J.*, **499**, 7.

Gyuk, G., Evans, N.W., Gates, E. I., 1998, *Ap. J.*, **502**, 29.

Kent, S.M., 1986, *A. J.*, **91**,1301.

Kormendy, J., 1990, in *Evolution of the Universe of Galaxies*,ed. R. G. Kron (Provo, UT; BYU Press), p. 109.

Kerins, E. J. 1998, *Astron & Ap.*, bf 328, 5.

Marley, M.S., *et al.* 1997, *Science*, **272**, 1919.

Näslund, M. andJörsäter, S. 1997, *Astron & Ap.*, **325**, 915.

Rand, R.J. Kulkarni, S.R. and Hester, J.J. 1992, *Ap. J.*, **396**, 97.

Reach, W. T. *et al.* 1995, *Nature*, **374**, 521.

Rice, W., Merrill, K.M., Gatley, I., Gillett, F.C., 1996, *A. J.*, **112**, 114.

Rudy, R.J., Woodward, C.E., Hodge, T., Fairfield, S.W., and Harker, D.E. 1997, *Nature*, **387**, 159.

Rupen, M.P., 1991, *A. J.*, **102**, 48.

Sackett, P.D., Morrison, H.L., Harding, P. and Boroson, T.A. 1994, *Nature*, **370**, 441.

Simard, L. and Pritchett, C. 1994, *A. J.*, **107**, 503.

Stevenson, D. J. 1991, *A.R.A.A.*, **29**, 163.

Trimble, V. 1987, *ARAA*, **25**, 425.

Vogler, A., Pitesch, W., and Kahabka, P. 1996, *Astron & Ap.*, **305**, 74.

This manuscript was prepared with the AAS LaTeX macros v4.0.

Table 1: Properties of NGC 4565

$\alpha(1950)$	$12^h33^m52^s$
$\delta(1950)$	26°15′47″
Orientation Angle	136° (E of N)
Galactic latitude	86°
Ecliptic latitude	27°
Distance	10.0[1] Mpc
Size (B=25 mag sec^{-2})	15.9′×1.85′
	49 kpc ×5.7 kpc
Integrated V brightness	10.4 mag
Sampling along minor axis	±4′, 6.8′, 17.2′
	±12, 20, 50 kpc

[1]Distance estimates range from 9.7 to 10.3 Mpc. (Simard and Pritchett, 1994). We adopt 10 Mpc.

Table 2: ISO Observing Log

B(1950)	ISO Observation*	Direction	B(1950)	ISO Observation*	Direction
Position: South-3	Scans: 1,2,3,4		Position:North-1	Scans: 1,2,3,4	
$12^h32^m59.0^s$	18401807[1]	N-going	$12^h34^m04.7^s$	18401810	N-going
26°04′18″	22100524	S-going	26°18′32″	22100521	S-going
50 kpc South	22100618	S-going	12 kpc North	22100615	S-going
on minor axis	22100701[1]	N-going	on minor axis	22100704	N-going
Position: South-2	Scans: 1,2,3,4		Position:North-2	Scans: 2,3,4	
$12^h33^m30.8^s$	18401808	N-going	$12^h34^m13.2^s$	18401811	N-going
26°11′11″	22100523	S-going	26°20′23″	22100520	S-going
20 kpc South	22100617	S-going	20 kpc North	22100614	S-going
on minor axis	22100702	N-going	on minor axis	not observed	
Position:South-1	Scans: 1,2,3,4		Position:North-3	Scans: 2,3,4	
$12^h33^m39.3^s$	18401809	N-going	$12^h34^m45.0^s$	18401812	N-going
26°13′02″	22100522	S-going	26°27′16″	22100519[1]	S-going
12 kpc South	22100616	S-going	50 kpc North	22100613[1]	S-going
on minor axis	22100703	N-going	on minor axis	not observed	

*CISP numbers include day number and a sequence number. Day 184 corresponds to 19/25/96; day 221 corresponds to 25/06/96.

[1]Rejected due to residual transient response.

Table 3: Measurements of NGC 4565 Halo

Position	Median Surface Brightness (Kjy sr^{-1})
South-3	-0.0 ± 2.8
South-2	1.2 ± 1.0
South-1	-1.8 ± 4.6
North-1	-4.8 ± 2.9
North-2	-1.8 ± 2.2
North-3	-1.0 ± 2.9
Avg. (N+S)-3	-0.5 ± 2.0
Avg. (N+S)-2	-0.3 ± 1.6
Avg. (N+S)-1	-3.3 ± 2.7

Table 4: Models for NGC 4565 Halo

Model	Mass ($M_\odot$)	α	N_* (10^{12})	$< M_* >$ ($M_\odot$)	L_* (10^9 $L_\odot$)	F_* (Jy)	I_ν(12 kpc) (KJy sr^{-1})	I_ν(20 kpc) (KJy sr^{-1})
1	0.2	–	1.8	0.2	9	0.72	51	23
2	0.07	–	5.0	0.07	0.03	0.01	0.8	0.4
3	0.02-0.2	1.0	2.6	0.13	7	0.70	49	23
4	0.02-0.07	1.0	7.0	0.05	0.015	0.005	0.34	0.16
5	0.7	–	0.5	0.7	1.5	0.006	0.41	0.18

Fig. 1.— A schematic map of the region around NGC 4565 showing the positions on the ON and OFF points. The galaxy is denoted by the blue light B_{25} mag sec^{-2} contour *Ken, can you put in an ellipse with 15.9x1.8 arcmin at 136 deg E of N?)* (Table 1).

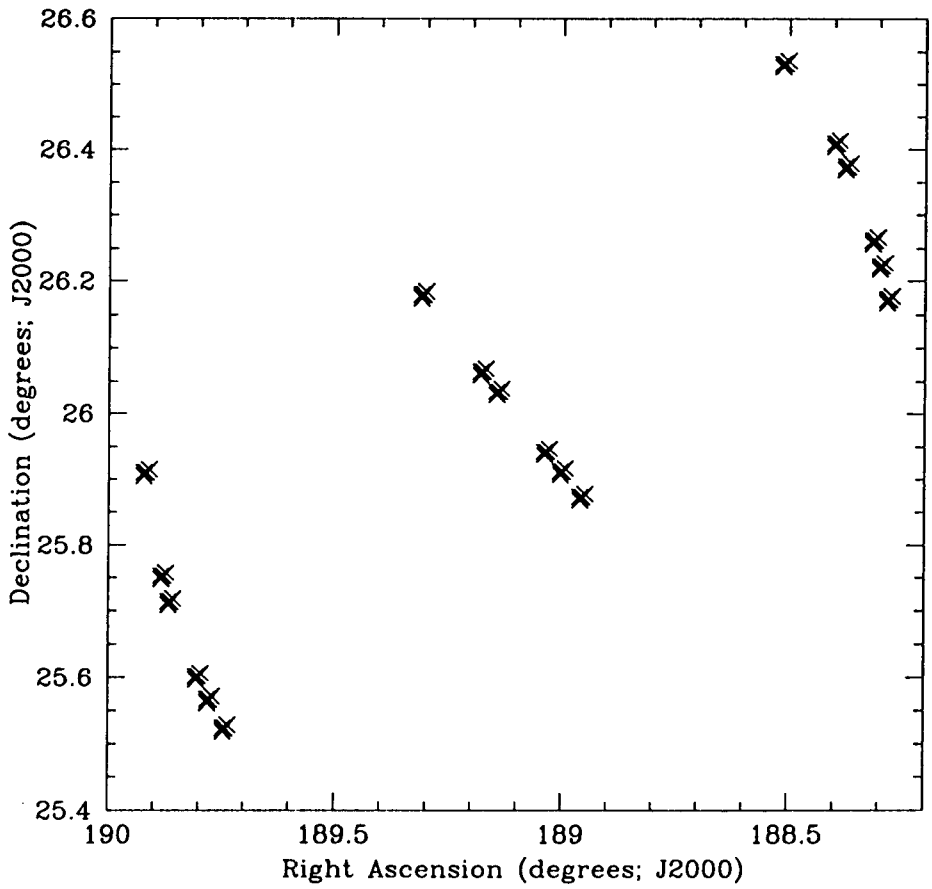

Fig. 2.— Median values of the fields as measured in each scan. Triangles correspond to the first "ON" field, squares to the first "OFF" field, pentagons to the second "ON" position, and hexagons to the second "OFF" position. Solid points correspond to the expected values according to a model for zodiacal thermal emission (Good 1994). Note that the sky position corresponding to a datum within each scan depends on the direction of the scan.

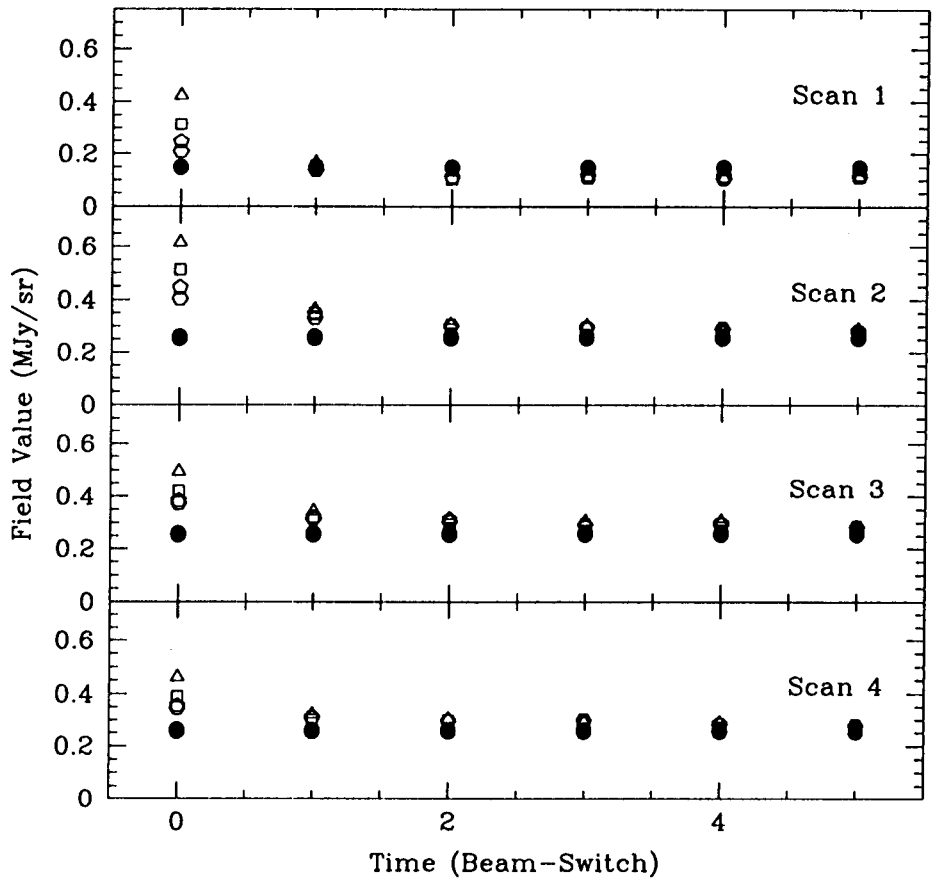

Fig. 3.— Difference between first and last stare at "on" field. Conventions are the same as in figure 2

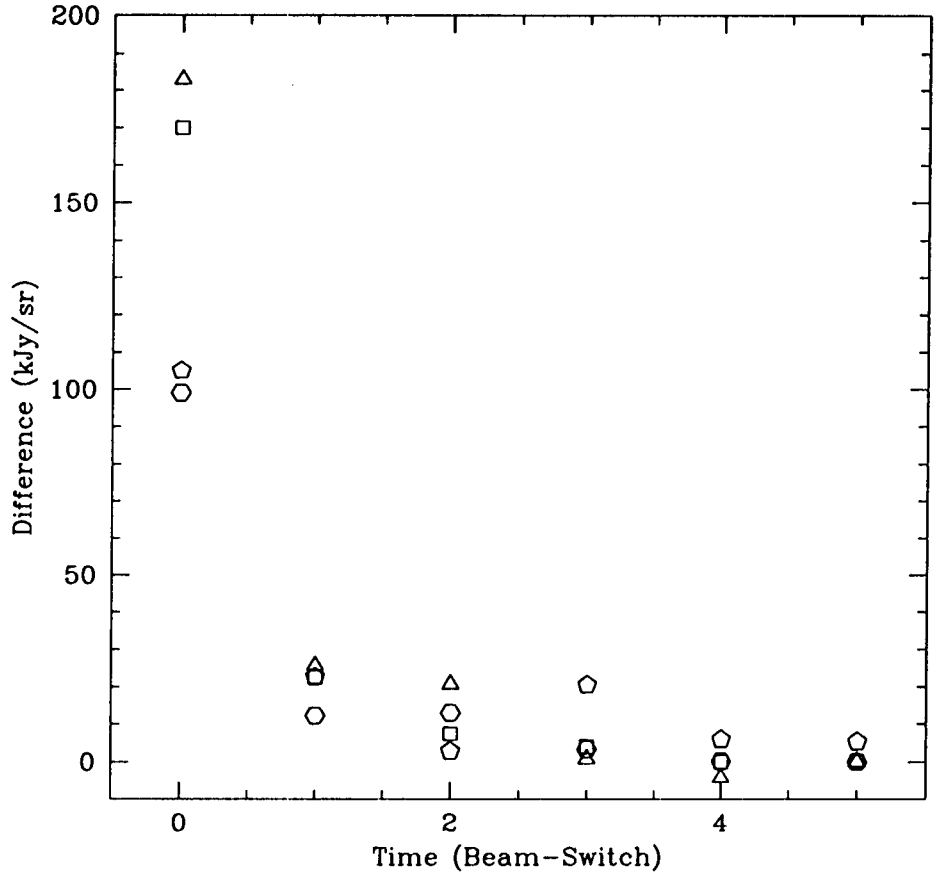

Fig. 4.— Zodiacal Differences. Top panel corresponds to scan 1, bottom panel to scan 4. Data are shown as crosses, model predictions as open circles.

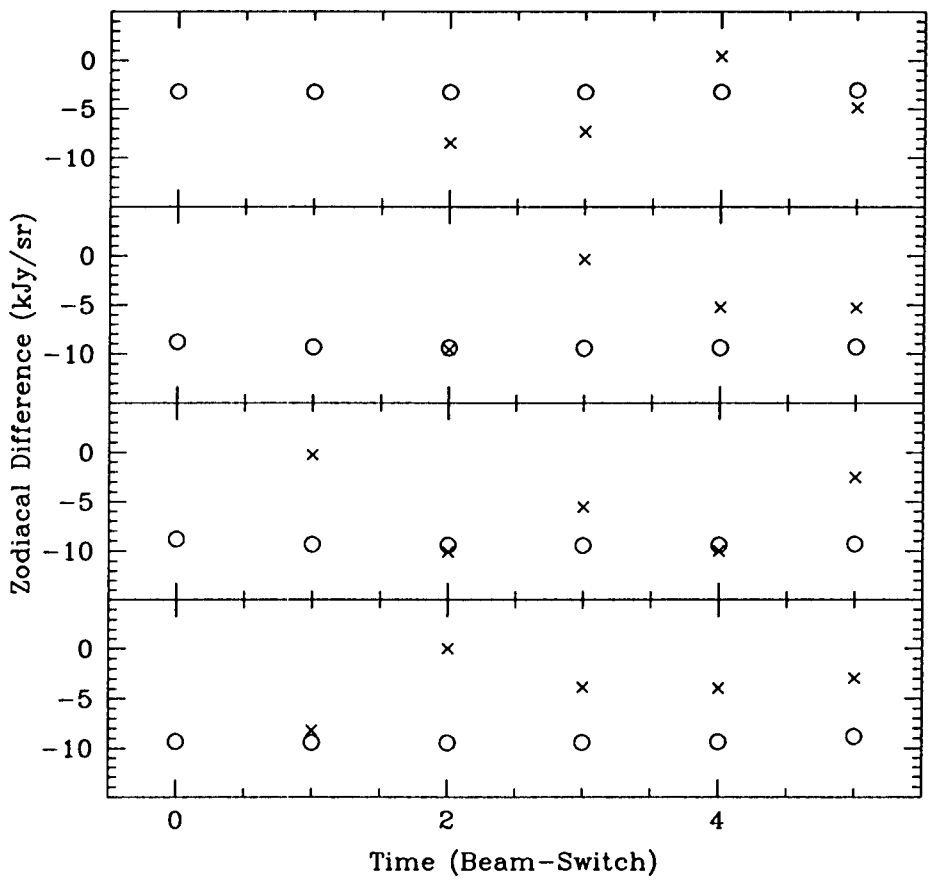

Fig. 5.— Triple Differences for data along each scan. Symbols denote: 1) second ON minus average of two OFFs (crosses) or average of two ONs minus average of two OFFs (boxes).

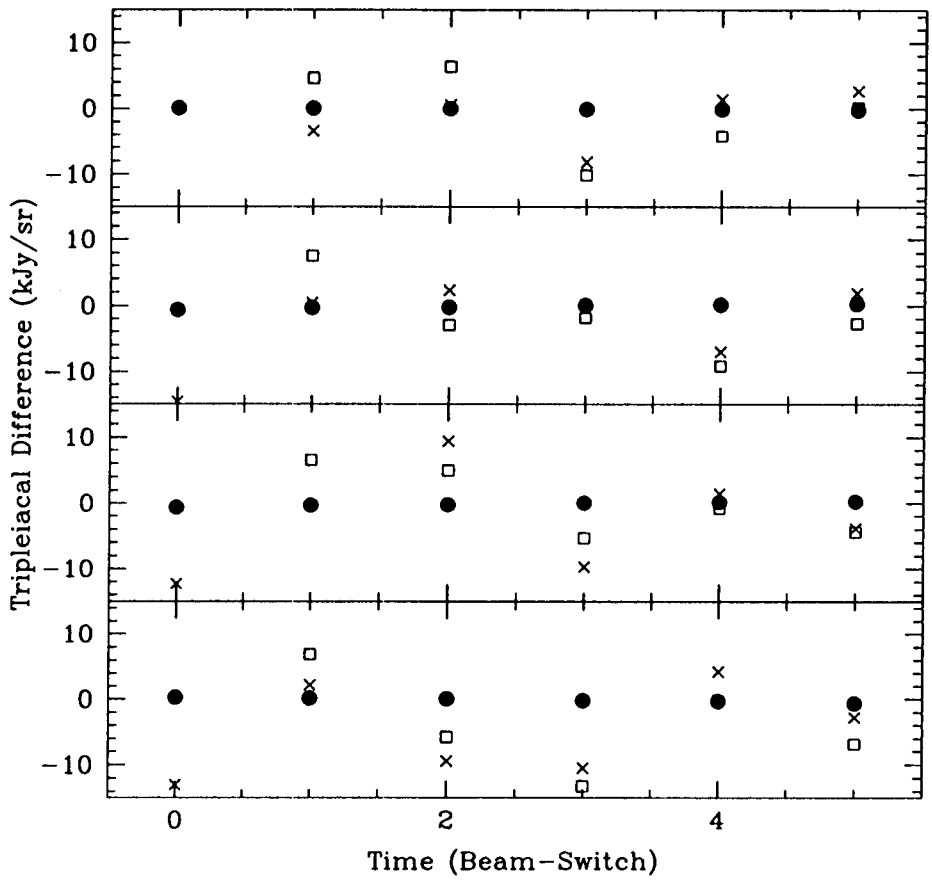

Fig. 6.— Science limits. Crosses correspond to first form of beam switch difference, boxes to the second. Error bars are one-σ. The points are offset from each other for clarity.

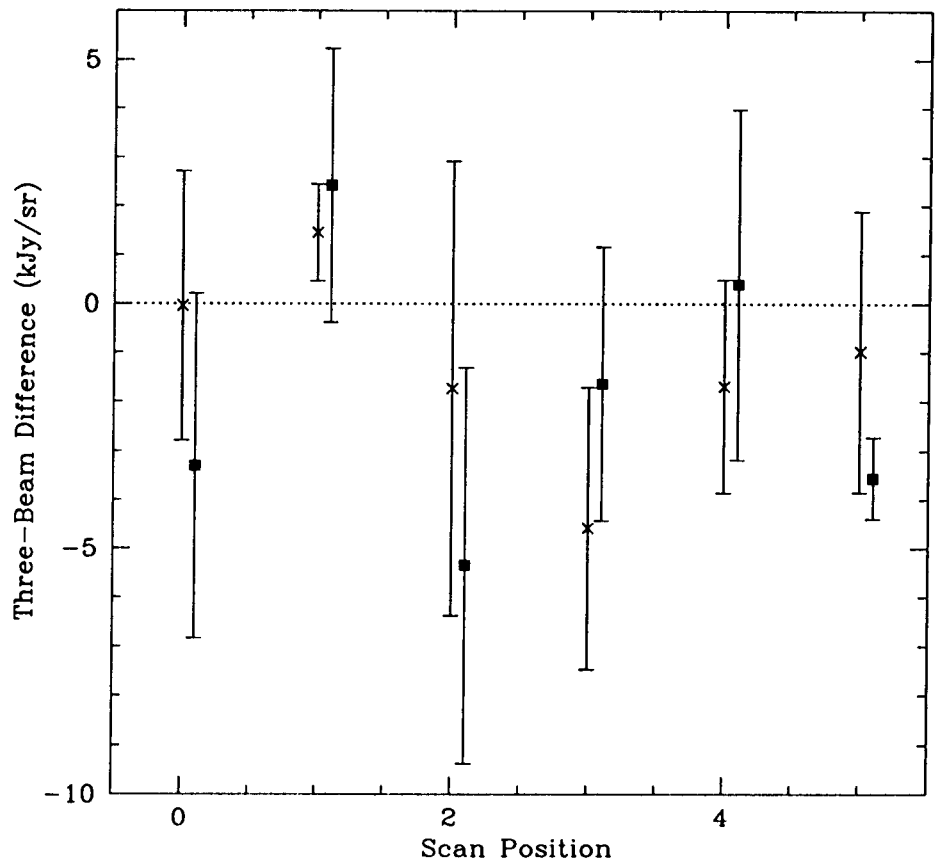

Fig. 7.— A number of models for the halo of NGC 4565 are shown as described in the text. The 3 σ ISO upper limits are shown as circles. From top to bottom the models are: 0.2 $M_{\odot}$stars (solid line) and almost on top of this curve a 0.02-0.2 $M_{\odot}$distribution (dash-dot); 0.07 $M_{\odot}$brown dwarfs (dashed line); white dwarfs (dash-dot-dot); 0.02-0.07 $M_{\odot}$brown dwarfs (dot-dot). The plus signs connected by a solid line denote the visible light data from Näslund and Jörsäter (1997) extrapolated to 4.5 μm.